Tectonophysics 873 (2024) 230217

Contents lists available at ScienceDirect

Tectonophysics

journal homepage: www.elsevier.com/locate/tecto

Unexpected postglacial faulting in passive continental margins: Storfjorden glacial trough, Barents Sea

María Teresa Pedrosa-González [a,*], Jesús Galindo-Zaldivar [a,b], Lourdes González-Castillo [a], Gemma Ercilla [c]

[a] Departamento de Geodinámica, Universidad de Granada, 18071 Granada, Spain
[b] Instituto Andaluz de Ciencias de la Tierra (CSIC-Universidad de Granada), 18071 Granada, Spain
[c] Marine Geosciences, Institut de Ciències del Mar, Consejo Superior de Investigaciones Cientificas (CSIC), 08003 Barcelona, Spain

ARTICLE INFO

Keywords:
Barents Sea
Passive continental margin
Glacial trough
Glacio-seismotectonic
Active reverse faulting

ABSTRACT

In high latitude continental margins, glacio-seismotectonics becomes particularly relevant during postglacial unloading periods and related isostatic rebound. Based on multibeam bathymetry and parametric profiles, an unexpected active 30 km long NNW-SSE fault is imaged for the first time in the inner Storfjorden glacial trough, at the passive continental margin of the Barents Sea. The 10 km southern tip of the fault was surveyed in detail and it is characterised by a total fault throw of 65 m. The fault forms an asymmetric valley with an upraised block to its east (top at 245 m water depth), a downthrown block to the west (at 310 m water depth), and a most recent fault scarp with 8 m relief at the seafloor valley axis. Recent fault activity is evidenced by its morphological expression on the seafloor, the faulting of the glacial, glaciomarine and marine sediments and streamlined landforms formed during the last glacial-interglacial period. Mass-flow deposits along the upraised block would also indicate recent fault activity.

This fault may trigger earthquakes of up to M_W 6.2, based on the magnitude/length ratio of the detailed surveyed segment, which is similar in magnitude to those that occurred in the nearby northeastern regions during 2008–2012. In any case, earthquakes may reach up to M_W 6.8 if the entire fault length is activated. Rather than the expected normal fault on the passive margin, this fault seems to be reversed and dipping eastwards. The integration of the Storfjorden glacial trough reverse fault with regional structures suggests that the fault activated the southwestward front of a wide, continental crustal block. These results are in accordance with a change in the stresses in the passive continental margin since the rifting stage, from extension to post-rift compression, and suggest that postglacial unloading may have favoured the fault development.

1. Introduction

The main tectonic structures observed on passive continental margins are inactive normal faults formed during continental rifting and followed by post-rift quiet subsidence (Brekke, 2000; Faleide et al., 2008; Ebinger et al., 2013). However, regional stresses transmitted through basement rock may later deform these margins and produce differential subsidence, exhumation and compressional faults and folds (Johnson, 2008). High latitude margins have undergone the tectonic effect of glacial isostatic adjustments (GIA), because glacial and interglacial cycles affect the thickness of the ice sheet (Lambeck et al., 2002a, 2002b). GIA processes represent the solid Earth response to changes in ice and ocean loadings throughout the glacial cycles. When ice sheets grow, the lithosphere flexes to accommodate the increased load, while ice loss results in uplift. The lithosphere mainly accommodates the load through elastic deformation during glacial cycles of loading and unloading, while the upper asthenosphere displays viscoelastic behaviour. The location of the grounding lines (Gomez et al., 2010) during the glacial cycles is also affected by the mantle rheological features that in certain settings may contribute towards stabilising the ice cap and grounding line location (Whitehouse et al., 2019). During the postglacial period, rapid isostatic rebound such as that which occurred during the Bølling Allerød (~ 14.800–12.700 ky) (Ingólfsson and Norddahl, 2001), provoked tilting and the rapid uplift of the crustal hinterlands and continental margins of the Arctic glaciomarine regions (Fjeldskaar et al., 2000; Clague and James, 2002).

* Corresponding author.
E-mail address: maytepedrosa@ugr.es (M.T. Pedrosa-González).

https://doi.org/10.1016/j.tecto.2024.230217
Received 8 September 2023; Received in revised form 30 December 2023; Accepted 18 January 2024
Available online 20 January 2024
0040-1951/© 2024 The Authors. Published by Elsevier B.V. This is an open access article under the CC BY-NC license (http://creativecommons.org/licenses/by-nc/4.0/).

In these glacio-tectonic scenarios, postglacial isostatic rebound is the main cause of fault reactivation and development of new faulting in the lithosphere due to postglacial unloading and the subsequent uplift. This setting leads to pronounced seismic activity that may cause submarine slope failure (Stewart et al., 2000; Watts, 2001; Maslin et al., 2004; Kukkonen et al., 2011; Pirli et al., 2021; Steffen et al., 2021). The rate of glacio-seismotectonic faulting decreases during the presence of an ice sheet and strongly increases during deglaciation due to the decrease in the average normal stress as has been proven by numerical modelling (Turpeinen et al., 2008; Hampel, 2017). Tectonic deformations have occurred at the Møre and Lofoten passive margins in Norway, simultaneous to a major Miocene regression (Løseth and Henriksen, 2005), and related to long-term-uplift along west and northern Norway (Japsen and Chalmers, 2000; Keiding et al., 2015 and references therein). During the earliest Holocene period, the glacial isostatic adjustment provoked the reactivation of reverse faults in Scandinavia (Turpeinen et al., 2008; Steffen et al., 2021), reaching a maximum towards the end of the period ~13–9 ka. In North America, fault reactivation is considered to have begun prior to 9 ka (Klemann and Wolf, 1998), whereas, reactivation of normal faults has occurred along the Wasatch Fault in Utah (Hampel and Hetzel, 2006).

Therefore, deglaciation provides a feasible glacio-seismotectonic mechanism for recent active faulting and seismicity in high latitude margins such as in the glacio-tectonic scenarios of the southern Svalbard Islands, in the northwestern Barents Sea. The Barents Sea and Svalbard were covered by extensive large ice domes (Fig. 1B) and developed large ice shelves (Vorren et al., 2011; Knies et al., 2009; Rebesco et al., 2014; Lasabuda et al., 2018) with rapidly retreating stages during the Holocene. The southern Svalbard islands were deformed by a fold-and-thrust belt limited by the Hoursund fault zone (HFZ), formed from Paleozoic to Tertiary that seems to be inactive today (Bergh and Grogan, 2003; Minakov et al., 2018). In southern Svalbard, the Storfjorden glacial trough is affected by a strike-slip seismicity that reached a magnitude of $M_W \sim 6.1$ in 2008, in southern Spitsbergen (Bergh and Grogan, 2003; Pirli et al., 2013). Furthermore, it has been proposed that earthquakes of up to $M_W \sim 8$ could occur in the western Barents Sea during deglaciation Arvidsson (1996). Thus, the remarkable seismicity in the western Barents Sea shows tectonic activity and calls for neotectonic fault analysis to link postglacial uplift with the development of new faults or the reactivation of pre-existing faults.

This study shows for the first time a striking active fault in the Storfjorden glacial trough located in the former passive margin. We analyse its morphological impact and deformation and its effect on the most recent stratigraphy and deposits, to characterise the fault activity and its potential seismicity. This research provides new evidence of glacial-seismotectonically induced faults and insights that help to determine its earthquake hazard in this region that has undergone periods of alternating transpression and extension, glacial or tectonically induced.

2. Regional setting

The Storfjorden Glacial Trough (StGT) is located in the continental margin of the northwestern Barents Sea, bounded to the west by the oceanic crust of the Greenland Sea, to the north by Svalbard, and to the south by the Spitsbergen Bank (Gabrielsen et al., 1990) (Fig. 1A and B). It has been excavated during the glacial periods by ice-streams fed by several ice domes (Pedrosa et al., 2011; Lucchi et al., 2015; Shackleton et al., 2019) (Fig. 1B). The StGT is a relatively medium-sized NE-SW glacial trough (within an area of 35,000 km^2) 272 km long and 130 km wide at the continental shelf break.

The western Barents Sea was deformed by the dextral shear displacement of Greenland (North American plate) with respect to Svalbard (Eurasian Plate) during the Paleocene-Eocene North Atlantic opening that developed the Greenland Sea (Talwani and Eldholm, 1977; Srivastava, 1985; Olesen et al., 2007; Engen et al., 2008; Faleide et al., 2008; Gaina et al., 2009; Lasabuda et al., 2018, 2021; Gac et al., 2020). The continental basement has undergone extensional, strike-slip and compressional episodes that develop a fold-and-thrust belt from the Paleozoic (Friend et al., 1997) up to Tertiary (Bergh and Grogan, 2003). This setting favoured alternating of episodes of transtension, strike-slip and transpression (Gac et al., 2020) during the development of fold-and-thrust belts.

After the rifting and development of the passive margins, seafloor spreading has occurred since the Miocene along the Knipovich Ridge (Engen et al., 2008; Dumais et al., 2021) resulting in the opening of Fram Strait (Fig. 1A) which led to deep-water circulation between the northeastern Atlantic Ocean and the Arctic Ocean (Faleide et al., 2008; Engen et al., 2008; Jakobsson et al., 2007; Jokat et al., 2019; Kristoffersen, 1990).

The Sørkapp-Hornsund (southern Spitsbergen) tectonic structures (Fig. 1B, C), located at the northwestern Barents Sea, were active during the Cenozoic (Vincenz et al., 1984; Dallmann et al., 1993; Dallmann, 1993; Winsnes et al., 1993; Bergh and Grogan, 2003). The Hornsund Fault Zone (HFZ) at the western shore off Spitsbergen and the Inner Hornsund Fault Zone (IHFZ) (Bergh et al., 1997; Gabrielsen et al., 1990, 1997; Bergh and Grogan, 2003; Faleide et al., 2015) belong to the West Spitsbergen fold-and-thrust belt (Fig. 1D) (Myhre and Eldholm, 1988; Faleide et al., 1991). Eastwards, the Billefjorden Fault Zone (BLF) and the Lomfjorden Fault Zone (LFZ) comprise of normal, reverse and strike-slip faults and limit the eastern Spitsbergen (Fig.1D) (Bergh and Grogan, 2003).

Svalbard is an important area for local intraplate seismicity. This seismic activity occurs mainly in two regions: (i) Heerland with low seismicity ($M_W < 2.4$) (Mitchell et al., 1990 and references therein); and (ii) the Storfjorden glacial through, where the highest earthquake magnitude of M_W 6.1 was recorded in 2008 (Pirli et al., 2013) (Fig. 1D). Moreover, in the Edgeøya platform, earthquakes of M_W 5.7 and M_W 5.1 occurred in 2003 and 2016 respectively, in the northern areas (Fig. 1D) (Stange and Schweitzer, 2004; Pirli et al., 2021). The world stress map (Heidbach et al., 2016) shows scarce data from the Barents Sea continental margin. Far south of the study area, reverse earthquake focal mechanisms indicate ENE-WSW compressional stress and roughly similar NE-SW compression is indicated by stress release from exploration wells.

3. Material and methods

High-resolution bathymetry and sub-bottom parametric profiles were collected from the mid sector of the StGT during the IPY Cruise SVAIS, on board the BIO Hespérides (Longyearbyen, July 29–August 17, 2007). Bathymetry was logged using the Simrad Mermaid system and data was processed using the CARIS HIPS & SIPS software (https://www.teledynecaris.com/en/products/hips-and-sips/), to perform morphological analysis, and create a high resolution (25 m) Digital Terrain Model (DTM). The parametric profiles were obtained using a Kongsberg TOPAS PS 18 hull-mounted parametric system, simultaneously with the above-mentioned multibeam echosounder. This system uses two primary frequencies, ranging from 16 to 22 kHz to produce a narrow beam with a secondary frequency ranging between 0.5 and 6.0 kHz. The dataset was sampled at 16 kHz and stored both in its raw proprietary format and the conventional SEG-Y format. They were subsequently imported into the IHS Kingdom Suite software (https://kingdom.ihs.com/) after a SEG-Y header edition. The conversion from two-way travel time to depth measured on the TOPAS profile was made using a sediment sound velocity equal to 1600 m/s (Pedrosa et al., 2011; Pedrosa-González et al., 2022).

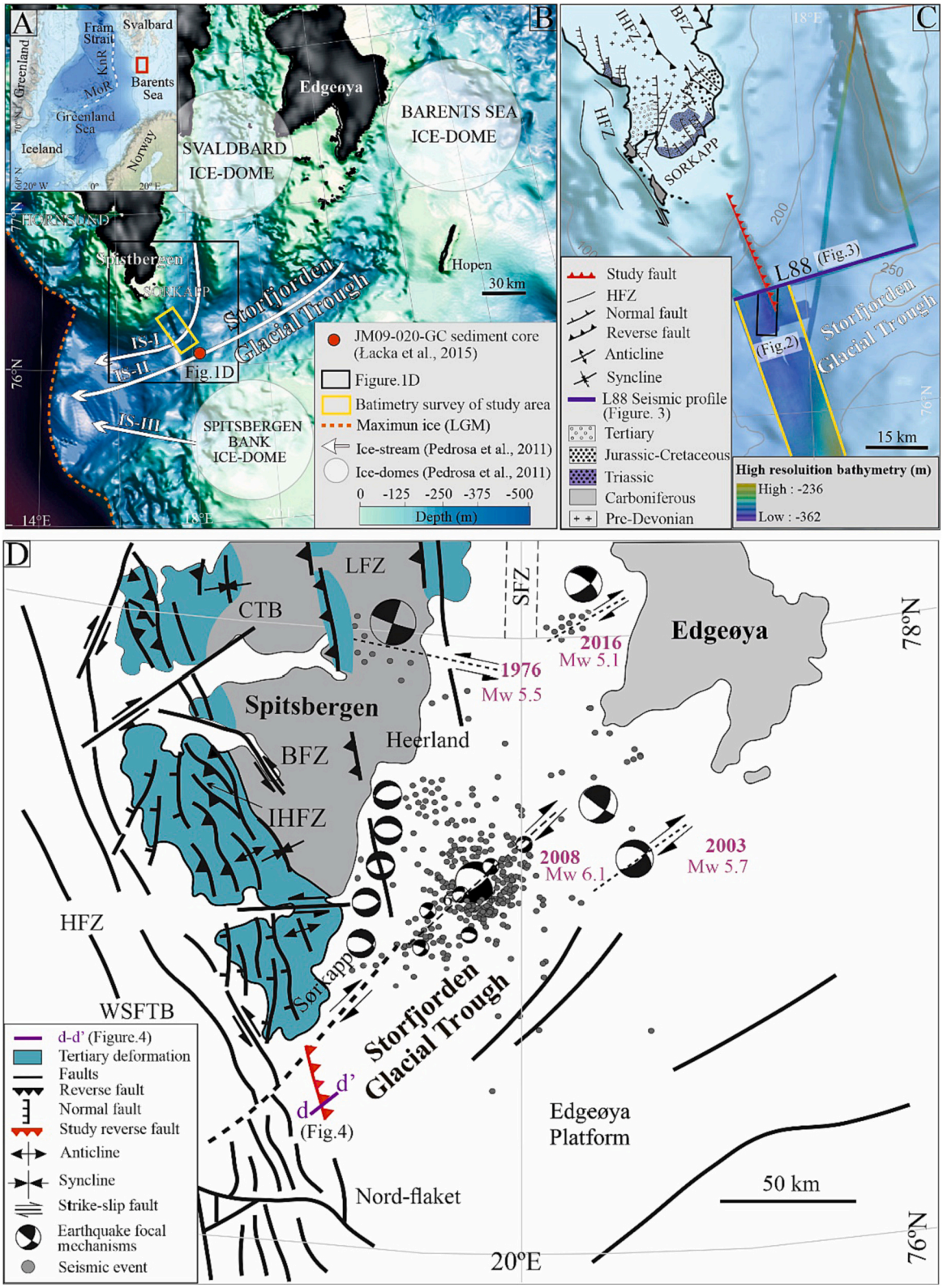

Fig. 1. Geological setting and seismicity of the Storfjorden glacial trough (StGT). A) Regional colour shade relief bathymetry map displaying the study area (red square). B) Shade relief map of the StGT (IBCAO) v3.0 (Jakobsson et al., 2012). C) Tectonic structures in the southern Spitsbergen and StGT (Bergh et al., 1997; Bergh and Grogan, 2003; Faleide et al., 2008, 2015; Lasabuda et al., 2018). D) Structural and seismicity map of southern Svalbard Islands and northwestern Barents Sea (Bergh et al., 1997; Bergh and Grogan, 2003; Faleide et al., 2008, 2015; Lasabuda et al., 2018). Earthquakes from Pirli et al., 2013, 2021. BFZ, Billefjorden Fault Zone; HFZ, Hornsund Fault Zone; IHFZ, Inner Hornsund Fault Zone; KnR, Knipovich Ridge; LFZ, Lomfjorden Fault Zone; MoR, Mohns Ridge; SFZ, Storfjorden Fault Zone. (For interpretation of the references to colour in this figure legend, the reader is referred to the web version of this article.)

4. Results

4.1. Seafloor multibeam morphology

The seafloor morphology of the mid sector of StGT (Fig. 2A) is characterised by a valley (5 km wide and up to 65 m of relief) that may reach up to 30 km in length (Fig. 1B, C). The tectonic nature of its formation and location seems to be controlled by a NW-SE linear feature extending >10 km (Fig. 2A). This feature is located on the valley floor and is characterised by an 8 m relief scarp that fades out towards the southeast. The valley displays an asymmetric V cross-section evolving to a U cross-section southeastward. The eastern wall is taller (65 m high) and steeper (3° decreasing to 1.5°) than the western wall (40 m high; gradient <1.5°). The seafloor walls are shaped by sedimentary features such as mass-flow deposits and glacial streamline landforms. The mass-flow deposits occur mostly in the steeper eastern wall. There, the bathymetry shows downsloping concave features that seem to draw lobate features in the lower parts. The streamline landforms are mostly mapped on the gentle western wall, although locally they also extend downwards to the valley floor where it is wider. They consist of quasi-parallel, linear features, ranging from ~0.5 to 1.5 km in length and are oriented SW-NE at an oblique angle to the main valley trend. Their cross-section profiles display subtle positive reliefs of a few metres, separated by troughs to a depth of 10 m (Fig. 2A, E).

The adjacent external margins of the valley also feature landforms. The western margin displays streamlines similar to the next valley wall, although with more subtle relief. The eastern margin is affected by iceberg ploughmarks. They are highly linear to slightly irregular depressions with different relief sizes (metric in scale). They are clearly concentrated in the shallower area where a roughly SW-NE orientation can be noted.

4.2. High-resolution sub-bottom stratigraphy: Acoustic facies and deposits

The high-resolution seismic profiles show three distinct stratigraphic features. From oldest to youngest they are as follows:

A highly reflective surface (i) acoustically defined by prolonged echoes. It bounds underlying indistinct deposits with opaque acoustic response and local discontinuous stratified facies (Figs. 2 and 3). Its profile is characterised by a mound shaped (5 km long and 50 m high) domain with an irregular appearance, located to the east of the tectonic valley (Fig. 3).

This high surface reflectivity is overlaid by two regional discontinuous and irregular juxtaposed units (ii) (each up to 20 m thick) of sediment with transparent facies and rough upper boundaries. Locally, in the valley (Fig. 2), that surface is overlaid by small-scale lenticular bodies (up to 1500 m long, 25 m thick). They are vertically and laterally stacked and distributed along the eastern wall and valley floor. These lenticular bodies comprise transparent facies with internal reflections of high amplitude that point to the occurrence of different sub-bodies (Figs. 2 and 3).

The transparent units and lenticular bodies are draped by a relatively thin (up to 3 ms or 5 m thick) and discontinuous transparent unit (iii) that makes up the surface sediment (Figs. 2 and 3). In the valley, the lateral continuity of this level appears interrupted or is under the scale resolution of the parametric system, mostly in the eastern wall and the scarp (Fig. 2). In the western wall, the draping level mimics the sub-bottom irregularities closest to the surface, that correspond to the streamline landforms as imaged by multibeam bathymetry (Fig. 2).

In the shallower area of the adjacent mound domain, it shows a spiky seafloor surface where iceberg ploughmarks mostly occur.

4.3. Tectonic deformations: A main near-surface fault

The tectonic deformation is imaged by the morphology and the faulting of the stratigraphic features (Figs. 2 and 3). The asymmetry of the valley is related to a main fault that cuts deep-lying surfaces and the overlying sediment until the seafloor. The fault related relief has a strikingly sharp fault trace located along the trough and an eastern upraised block. Eastwards (Fig. 3), the undulated topography may be related to long wavelength folding or alternatively, may have glacial origins. Regional (Fig. 1C) and local detailed bathymetry (Fig. 2A) show that the fault has a straight trace with a NNW-SSE orientation. Its length is 30 km in the regional bathymetry (Fig. 1B), whereas the local survey covers the southern 10 km (Fig. 2A), where the total throw reaches 65 m and the recent throw in the fault scarp is up to 8 m.

5. Discussion

5.1. Recent sedimentation: constraining the time frames

The advance and retreat of glaciers due to glacial and interglacial periods provoke the erosion of pre-existing sediments (Boulton, 1979; Alley et al., 2019; Patton et al., 2022). Because of that, the near-surface sediments of the continental shelf and fjords generally correspond to the last glacial-interglacial period (Elverhøi et al., 1998; Ottesen et al., 2007; Knies et al., 2009). The analysis of the recent seismic stratigraphy and the multibeam seafloor morphology allow us to infer the history of recent sedimentation processes on the StGT. In this regard, based on the morphological and acoustic characteristics of the deep-lying highly reflective surface, the acoustic response of the underlying deposits and by comparison with the characteristic stratigraphic signature in other similar sedimentary contexts, we suggest that this surface represents the top of till-deformed deposits (Rebesco et al., 2011; Rüther et al., 2012; Bjarnadóttir et al., 2014; Bjarnadóttir and Andreassen, 2016; Lucchi et al., 2015; Zecchin and Rebesco, 2018; Shackleton et al., 2019). Thus, these sediments were deposited by the subglacial action of the ice-sheet (Alley et al., 1989; Ercilla et al., 1998; García et al., 2009) moving along the StGT during the last glacial period. The irregular morphology of that surface may result in subglacial processes such as deformation, ploughing and lodgement or a combination of these processes (Piotrowski et al., 2006; Dowdeswell and Hogan, 2016; Evans, 2017; Wise et al., 2017; Ottesen and Dowdeswell, 2022). The overlying two units and small lenticular bodies with their transparent acoustic character allow for penetration of the signal from the parametric system, thus suggesting they are made up of relatively fine and homogeneous sediments. In the glacial trough environment, fine sediment deposits commonly occur from suspension settling, release of sediment from gravity flows at grounding line from the melting ice, and sediment mass-wasting in the form of mass flows (Powell and Domack, 2002; Bjarnadottir et al., 2013). The regional distribution and variable thickness of the two units suggest their deposition from melting sediment gravity flows. They probably formed close to the grounding line as indicated by their spiky, rough upper surface, probably also due to further iceberg scouring (Wise et al., 2017). On the other hand, the small stacked lenticular bodies at the valley wall and floor are interpreted as mass-flow deposits resulting from gravitational sedimentary instabilities due to the overstepping (to 3°) of the upraised block. Sediments here as delivered and deposited from the ice base or grounding line would move downslope the block wall and redeposit mainly by mass flows.

In this scenario, the streamline landforms affecting the fault valley may be interpreted as gullies or sedimentary ridge-trough features. These gullies, that in glaciomarine environments are commonly formed by gravity flows of ice meltwater sediment (García et al., 2009; Ercilla et al., 2021 and references therein), have been discarded because their pathway does not fit with the direction of the maximum slope as followed by those flows. This means that the gullies' trajectory should be perpendicular to the regional slope rather than the oblique trend displayed. Discarding this genesis, the streamline landform formation may be interpreted in conjunction with the mass-flow deposits, whose distribution occurs mainly along the valley walls. This feature association would be tentatively interpreted in terms of variation in acceleration of

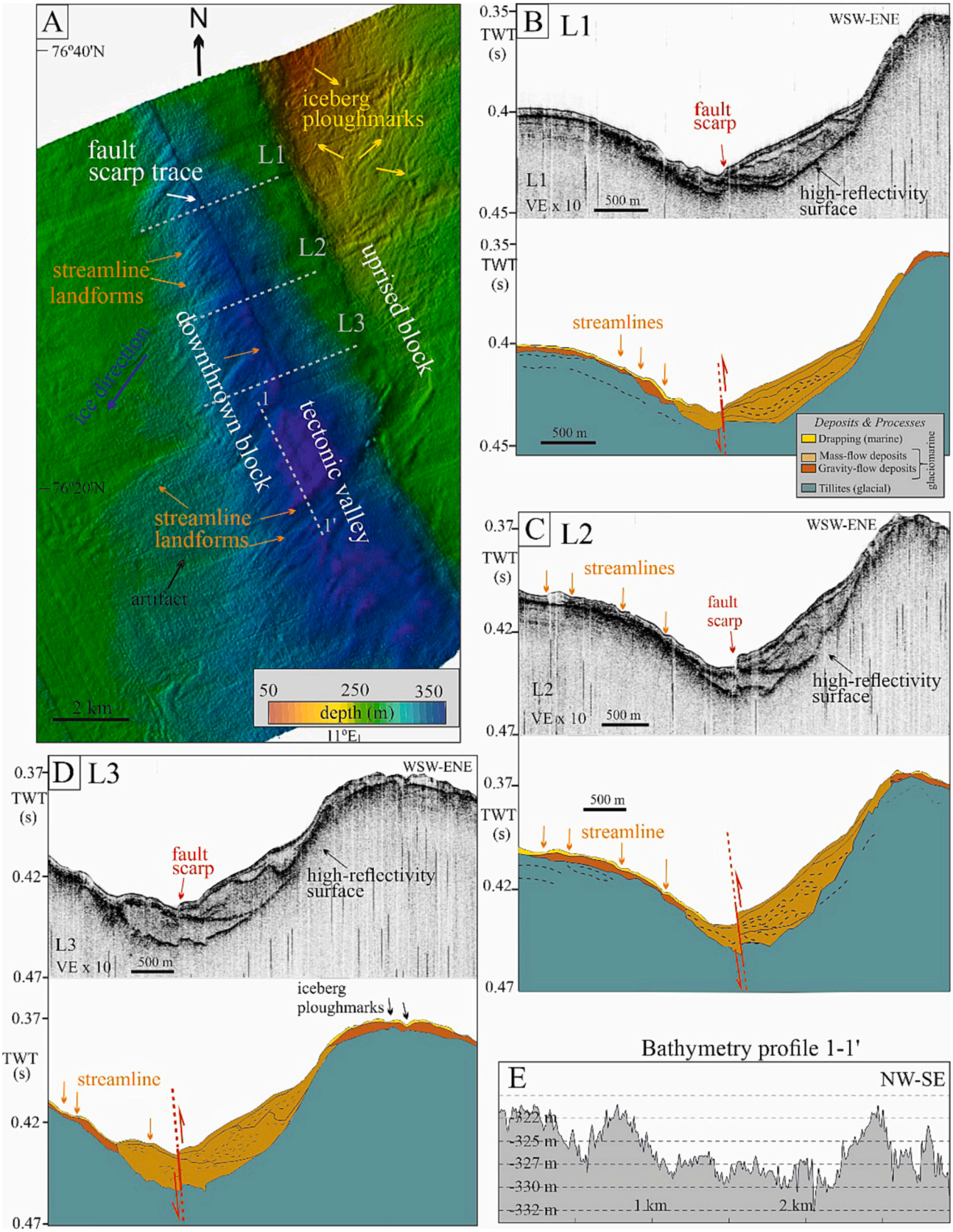

Fig. 2. Morphology and seismic stratigraphic features of the tectonic valley. A) Colour shade relief multibeam bathymetry map displaying the main morphological features, both tectonic and sedimentary in origin. B) to D) Parametric profiles (VEx10) show the main stratigraphic features defining the most recent sediments (glacial, glaciomarine and marine deposits). E) Topographic profile of the streamline landforms. Parametric profile locations are shown in Fig. 2A.

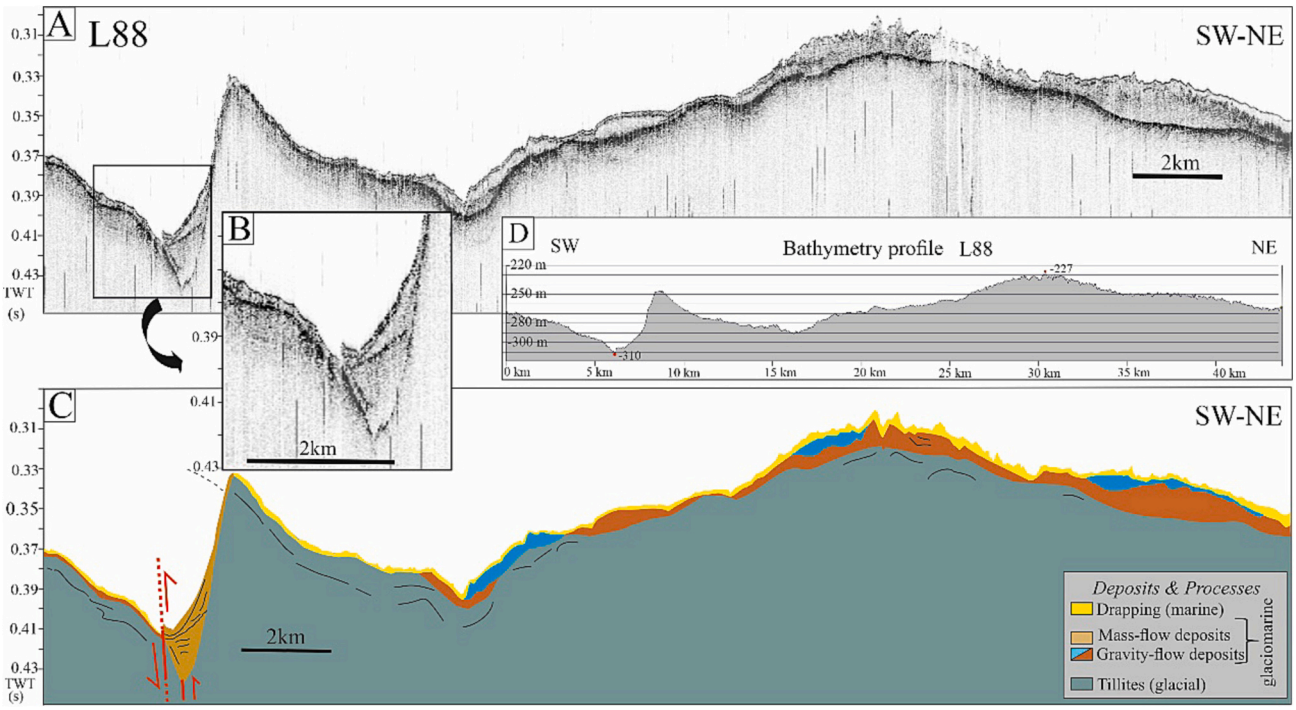

Fig. 3. Recent parametric stratigraphy based on L88 seismic profile. Location of parametric profile in Fig. 1C. A) Parametric profile (VE x10). B) The fault in the valley axis is zoomed. C) Line drawing displaying the main seismic stratigraphic features that characterise the most recent sediments of the tectonic valley and nearby area. D) The topographic profile based on multibeam bathymetry.

the ice movement during the pulsed episodes of still stands and advances as characterised by the last interglacial (Lønne and Nemec, 2011; Bjarnadottir et al., 2013; Dove et al., 2017). Commonly, ice over topographic highs as banks are slower, contrasting with a faster flow in troughs (Wellner et al., 2001). Furthermore, the glacial lineations are commonly indicative of ice ground acceleration (Boulton and Clark, 1990; Winsborrow et al., 2010; Stokes et al., 2013). Our tentative interpretation is that the effect of ice-anchoring as generated by the upraised fault block would have favoured a slower-moving ice flow, dumping subglacial material over its overstepping wall, and provoking the formation of mass flows or their subsequent mass wasting in the form of mass flows as has been mentioned above. Similar cases of ice anchoring have been described in Disco Bay (Greenland) where the troughs appear affected by fault steps that provide stabilising pinning points counteracting the retreat of the ice margin (Hoffman, 2016). The western StGT is also affected by the southern tip of Spitsbergen and underlying bedrock ridges, which provide lateral and basal pinning points thus stabilising the retreat of the ice stream (Shackleton et al., 2019). Once the ice has passed the upraised block and flowed over the gentle seafloor of the downthrown block, the ice flow accelerates forming the subglacial lineations. On the other hand, these lineations could be also interpreted as glacial elongated ridge-trough features, formed where ice has flowed over relatively softer sediment (Wellner et al., 2001). Slower-moving ice over the upraised block, followed by a longer period of ice coverage, would have favoured a higher over consolidation than the sediment on the downthrown block, which would be more easily eroded by the ice (Dowdeswell et al., 1993; Stokes and Clark, 2003; Bjarnadóttir and Andreassen, 2016; Batchelor et al., 2019).

Finally, the most recent thin unit draping the area would indicate more open-marine conditions. It would have been deposited by rain out of terrigenous particles coming from turbid meltwater plumes overflowed by tidewater glaciers and biogenous particles (Powell and Evans, 1983; Pfirman and Solheim, 1989; Chauché et al., 2014). This uniform blanket unit appears to be reworked by iceberg keels as suggested by multibeam imaging displaying iceberg ploughmarks (Fig. 2). Their improved development in the shallower area of the external margin and the fact that they show a roughly SW-NE trend and not a chaotic pattern, point to topographic control in the iceberg drifting (Jakobsson et al., 2011).

5.2. *Active tectonic deformations on the former extensional passive margin*

The rifting of the North Atlantic occurs in a setting of dextral displacement between southwestern Barents Sea and Greenland during Paleocene-Early Eocene (Lasabuda et al., 2018). The continental rifting and the development of the former extensional passive continental margin in the southwestern Barents Sea due to transtension is simultaneous to the contraction and transpression that develop the main faults and folds, both in the onshore southern Spitsbergen (Bergh and Grogan, 2003; Faleide et al., 2008) and offshore (Lasabuda et al., 2018) (Fig. 1D).

Since the mid-late Eocene, rifting and oceanic spreading has progressed northwards separating Greenland from the West Spitsbergen fold and thrust belt. Horsound Fault Zone (Fig. 2) in the offshore study area was considered a westward dipping reverse fault zone during Paleocene-Eocene, later affected by extension and becoming inactive before Pleistocene (Lasabuda et al., 2018). In any case, the most recent tectonic deformation remains unknown in the nearby StGT.

This contribution reveals for the first time the presence of a main NNW-SSE active fault on the southwestern Barents continental margin (Figs. 1, 2 and 3). This recent activity can be evidenced by: i) the scarp relief of this fault trace at the seafloor; ii) the vertical offset of the most recent glacial, glaciomarine and marine sediments; and iii) the potential mass-wasting of sediments in the form of mass flows due to the overstepping (to 3°) of the upraised block. The seismicity in the Edgeøya platform (Fig. 1D) reveals the presence of active NE-SW highly dipping dextral faults crossing the platform. WNW-ESE sinistral faults also occur in the Heerland area (Bergh and Grogan, 2003; Pirli et al., 2013). Moreover, earthquake focal mechanisms along the eastern coast of Spitsbergen Island indicate E-W normal faulting, supporting a roughly N-S extension. Junek et al. (2014) analysed the Edgeøya platform earthquake focal mechanisms and determined that close to our study

area, there is homogeneous ENE-WSW horizontal compression. This trend is oblique to the expected southeastwards regional displacement of Eurasia with respect to the North American plates derived from the NUVEL-1 model.

Extensional faulting usually occurs during the interglacial isostatic rebound (Hetzel and Hampel, 2005; Paxman et al., 2017). Earthquake focal mechanism data evidences that our study area undergoes a present-day N-S to NNW-SSE extension simultaneous to an orthogonal ENE-WSW compression (Junek et al., 2014), in agreement with the results far south as evidenced by the World Stress Map (Heidbach et al., 2016). This setting may be a consequence of the interaction of the ENE-WSW tectonic compression produced by the push of the Knipovich Ridge and the extensional setting related to the isostatic rebound.

The regional tectonic scenario considered together with the geometry and orientation of the active fault hereby mapped allows discussion of the fault kinematics (Fig. 4). The curved structure of the upraised and the downthrown fault blocks may constitute fault-related folds compatible with a curved fault surface, but this geometry is not significant to reveal their normal or reverse character (Brandes and Tanner, 2014). The fault may be considered a listric normal fault (Fig. 4B) dipping westwards and related to a reactivation of the former normal faults as developed in the continental margin during the *syn*-rift deformation. A similar character has been described by Lasabuda et al. (2018) for the Horsound Fault Zone which was only active up to the Paleocene. However, the local stress regime (Junek et al., 2014) points to ENE-WSW compression that disagrees with the expected extension as related to a NNW-SSE normal fault, but which better fits with its reverse character. Moreover, considering a relatively high-angle reverse fault dipping eastwards, better supports the detailed interpretation of parasound profiles (Figs. 2 and 3), despite the high vertical exaggeration. The eastwards tilting related to the shallow regional seafloor level of the upraised block, also fits with an eastward dipping reverse fault whose hanging wall has been dismantled by mass flow processes (Figs. 4A and 5). Although the data do not allow to precise exactly the fault dip, it should be a high-angle fault because the straight character of the fault trace. In fact, the presence of reverse faulting with the fault scarp reaching up to 30 m is a common glacio-seismotectonic feature (Stewart et al., 2000). Furthermore, the recently characterised reverse fault, may represent an incipient frontal ramp of a southwestward displacing block of Edgeøya platform on the continental margin, bounded by a dextral fault zone to the north (Fig. 5).

The onset of fault activity is difficult to be determined in detail with the currently available data. It should be evidenced by the change in the sediment thickness and the occurrence of mass-flow deposits. The gravity-flow deposits (Fig. 4, orange unit) fill concave gaps on the sea bottom, and they are absent in the upraised block close to the main fault, indicating a possible initial uplift simultaneous with deposition. According with ages of sediment core JM09–020-GC (Łącka et al., 2015),

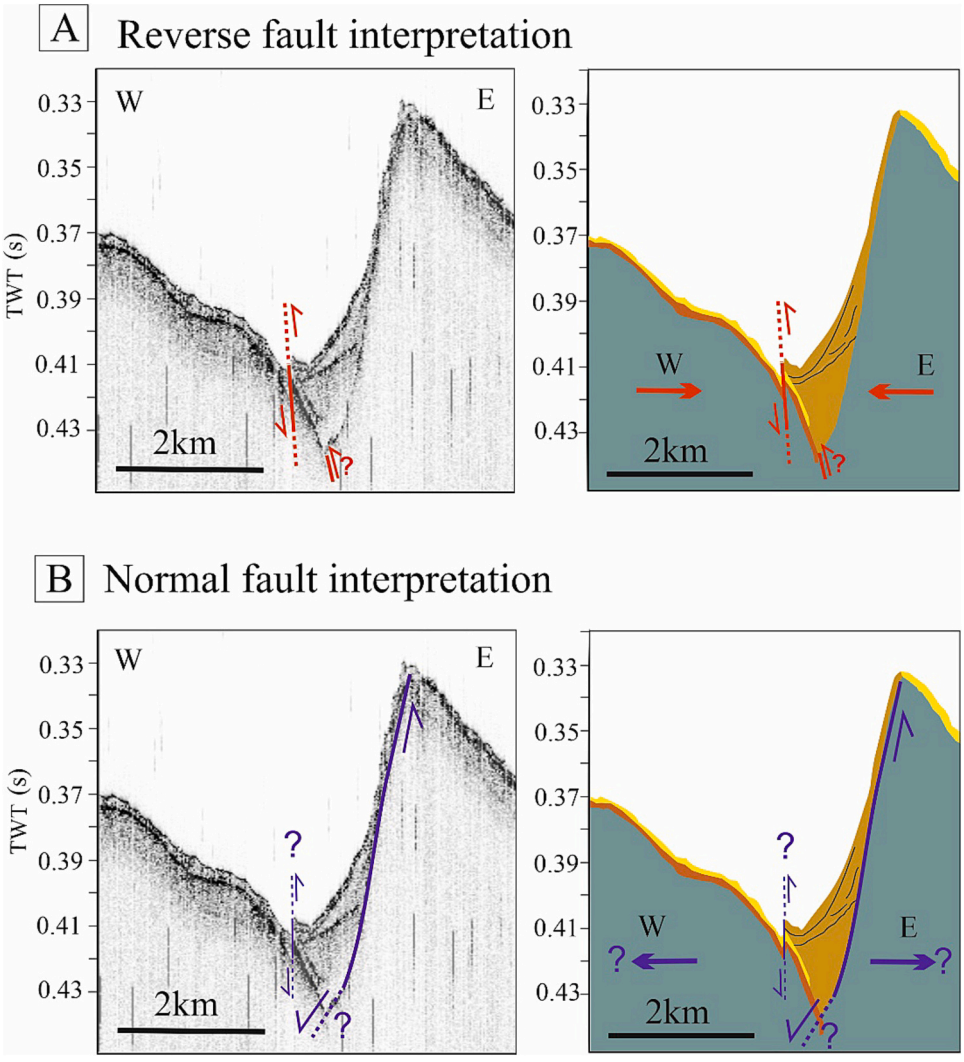

Fig. 4. Alternative interpretations of the parametric profile L88 crossing the tectonic valley, if considering the fault as reverse (A) or normal (B). Profile in Fig. 3. Uninterpreted image in Fig. 3B. Legend as in Fig. 3.

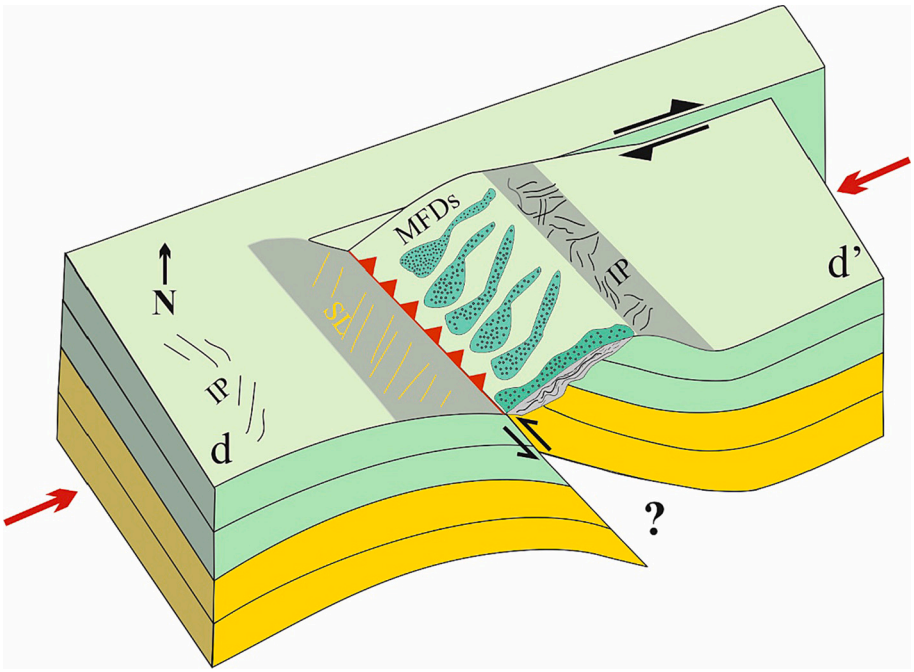

Fig. 5. Block diagram of the geodynamic context of the reverse fault. The fault would be related to the WSW displacement of a tectonic block bounded northwestward by an active seismic dextral fault zone. See Fig. 1 for the geodynamic context and location (Fig.1D) of the d-d' cross-section.

we estimate that the main fault could have originated since the termination of the Bølling–Allerød (13,950 cal yr BP) coinciding with the retreat of the Svalbard-Barents Ice Sheet. These data suggest that faulting is primarily a result of postglacial deformation, although the possibility of reverse faulting initiated during the glacial period due to tectonic compression from ridge push cannot be entirely ruled out. The main fault likely experienced subsequent periods of high activity, causing recent landslides that cover the valley, overlaying mass-flow deposits, and partially affecting the draping marine deposits. Moreover, the fault marked by a sea bottom scarp cuts through the gravity-flows unit and causes a minor variation in the thickness of the draping marine deposits (Fig. 4), supporting evidence of Holocene activity.

During the retreat of the last ice sheet in the post-glacial stage, the glacio-seismotectonic processes result from the activation of tectonic structures induced by changes in stresses due to postglacial unloading and the isostatic rebound (Gregersen et al., 1989; Turpeinen et al., 2008) (Fig. 6). The withdrawal of the last ice sheet in the Storfjorden glacial trough during the last deglaciation (Łącka et al., 2015; Nielsen and Rasmussen, 2018; Lasabuda et al., 2018) would have led to a decrease in the confining normal stresses and subsequently, the differential stress related to the tectonics would have reached the rupture point (Fig. 6). If horizontal compressional stresses are predominant due to the push of Knipovich Ridge, reverse faulting develops (Anderson, 1951). The newly defined recent fault develops parallel to the previous bedrock faults of the Cenozoic fold and thrust belt of the Inner Hoursund Fault Zone (Bergh et al., 1997; Gabrielsen et al., 1990, 1997; Bergh and Grogan, 2003; Faleide et al., 2015). Although this fault may have developed as a reactivated structure similar to those described by Lagerbäck and Sundh (2008) and Brandes and Tanner (2014), however, if it is considered a westward vergent reverse fault, it can be regarded as a new fault.

5.3. Fault seismic potential

Postglacial activation of the main fault zones in Svalbard and the northwestern Barents Sea may generate large earthquakes nowadays (Pirli et al., 2013). In Arctic areas, faults may reach trace lengths of up to hundreds of kilometres with estimated earthquakes of Mw $\geq$ 8 (Arvidsson, 1996; Lagerbäck and Sundh, 2008; Lindblom et al., 2015; Malehmir et al., 2016). The historical earthquake record for the Storfjorden glacial trough area shows that the highest magnitudes (Mw $\sim$ 6.1) occurred in 2008 and relevant earthquakes ($<$ Mw 5.7) also arose on the Edgeøya platform (Pirli et al., 2021). The magnitude/length ratio relationship as established by Wells and Coppersmith (1994) is widely used in literature also for submarine faults (Estrada et al., 2021) to assess the potential magnitude of earthquakes. In our study fault, the magnitude/length ratio relationship (Wells and Coppersmith, 1994) suggests maximum magnitudes of up to Mw $\sim$ 6.8, if the whole 30 km reverse fault is activated or Mw $\sim$ 6.2 if only the southwards 10 km long detailed surveyed segment is active, whether it is a normal fault or a reverse fault. These magnitudes are of the same order as those reported by the seismicity in the eastern regions (Pirli et al., 2021), although the study faulted area does not show evidence of any remarkable present-day seismic activity. The absence of seismicity may be related to the accumulation of stresses during the seismic cycle, although creep cannot be discarded. The 8 m fault scarp must have been formed by several events, because if its formation was due to a single event, it would represent an earthquake of Mw $\sim$ 7.3, according to Wells and Coppersmith (1994), a higher magnitude than the maximum magnitude that could have produced this fault considering its length (Mw $\sim$ 6.8). Taking into account the presence of large ice domes in the study area during the Last Glacial Maximum (LGM) (Fig. 1), the earthquakes associated with this fault could have caused sea-ice collapse, contributing to the rising sea level. In this framework, this fault may represent a tsunamigenic source to be considered in the future for detailed studies of the region.

6. Conclusion

An active fault is identified on the Storfjorden glacial trough, in the Barents Sea passive continental margin, where normal extensional syn-rift faults, sealed by post-rift sequences are expected. The fault has a NNW-SSE orientation, a length of 30 km, of which the 10 km southern part was surveyed in detail, and its recent activity is confirmed by morphological, stratigraphic, and sedimentary evidence. Morphologically, the fault forms an asymmetric valley with a 65 m uplift of the eastern upraised block and a striking seafloor linear fault scarp of up to 8 m high parallel to the valley axis. The fault cuts the streamline

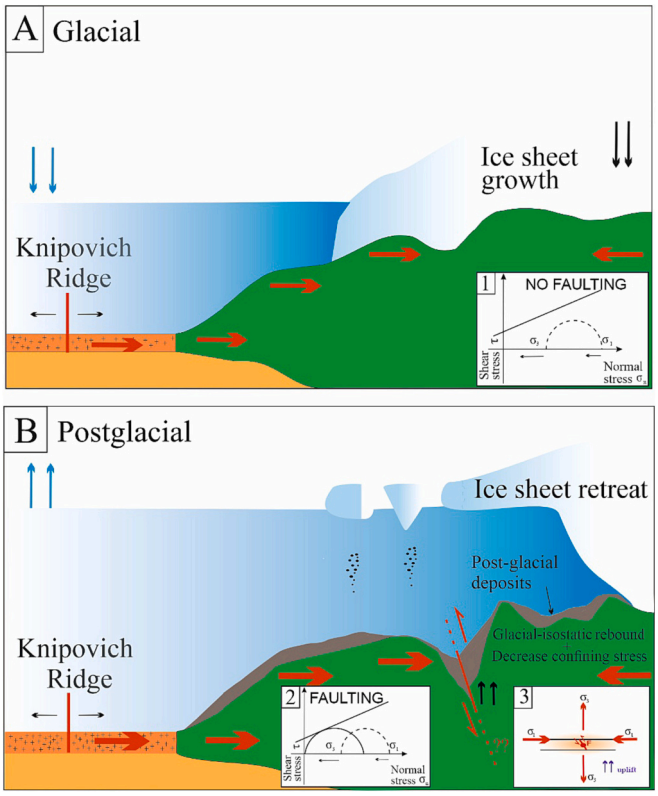

Fig. 6. Development of glacially triggered faulting in passive continental margin.
A) Glacial period without faulting. B) Interglacial period with reverse faulting during isostatic rebound (Turpeinen et al., 2008) by horizontal compression (large red arrows) related to Knipovich Ridge push. Glacio-seismotectonic faulting occurs due to the decrease of normal confining stresses during post-glacial unloading and therefore, the crustal differential stresses reach the rupture: 1) Mohr diagram during glacial period; 2) Mohr diagram illustrating the changes in the crustal stress field in a region from glacial to interglacial-current period. Mohr circle shifts to the left and intersects the Mohr–Coulomb failure envelope; 3) Sketch of stress during reverse fault activity.

landforms features and the most recent sediment made of glacial (till-ites), glaciomarine (mass-flow deposits) and marine (sediment settling from suspension) deposits from the last glacial-interglacial period. The mass-flow deposits may have also resulted from the mass-wasting due to the high slope gradients (up to 3°) of the eastern upraised block. This fault may produce earthquakes up to a magnitude of Mw 6.2 if the southern detailed surveyed segment is active, and up to Mw 6.8 if the full length is active.

The regional ENE-WSW tectonic compression determined by the seismicity fits better with a high-angle reverse east-dipping fault than with a normal west-dipping fault. This setting suggests that the continental margin has evolved from an ENE-WSW extension during rifting to an ENE-WSW tectonic compression, probably related to the push of oceanic spreading that occurs on the Knipovich Ridge. This fault may have been triggered by glacio-tectonic processes, by which the deglaciation decreases the confining stresses and differential stresses reach the rupture point. In this setting, the block upraised by the fault may have contributed to the anchoring of the ice stream in the northern Storfjorden glacial trough and may have affected iceberg drifting as suggested by the location and trend of iceberg ploughmarks.

This work underlines that it is essential to evaluate the geometry, kinematics, and maximum expected magnitude of glacially induced faults to mitigate the geological hazard of earthquakes in the Arctic areas. Glacio-seismotectonic in high latitude margins may have implications for long-term seismic hazards affecting offshore infrastructures.

CRediT authorship contribution statement

María Teresa Pedrosa-González: Writing – review & editing, Writing – original draft, Visualization, Validation, Supervision, Software, Methodology, Investigation, Funding acquisition, Formal analysis, Data curation, Conceptualization. **Jesús Galindo-Zaldivar:** Supervision, Investigation, Funding acquisition, Formal analysis, Data curation, Conceptualization. **Lourdes González-Castillo:** Writing – review & editing, Writing – original draft, Visualization, Validation, Supervision, Formal analysis, Data curation, Conceptualization. **Gemma Ercilla:** Writing – review & editing, Writing – original draft, Visualization, Validation, Supervision, Methodology, Investigation, Funding acquisition, Formal analysis, Data curation, Conceptualization.

Declaration of competing interest

The authors declare that they have no known competing financial interests or personal relationships that could have appeared to influence the work reported in this paper.

Data availability

The authors are unable or have chosen not to specify which data has been used.

Acknowledgements

We thank the comment of Dr. Tiago M. Alves, Dr. Yanghui Zhao, Dr. Holger Steffen and Dr. Karsten Gohl and the editor Dra. Claire Currie, that have improved the presentation and discussion of this contribution. We also thank all scientists and crew who participated in seagoing activities to obtain geophysical data in the framework of the SVAIS cruise. The authors wish to acknowledge the cooperation of Captain Pedro Luis de la Puente García-Ganges (BIO Hespérides) and of the technical staff at the UTM (Unidad Tecnología Marina; Consejo Superior de Investigaciones Científicas, CSIC, Barcelona). Finally, we acknowledge Asier Madarieta and Victor Tendero for general comments. This research was supported by Spanish IPY projects SVAIS (no. POL2006-07390/CGL) and IPY-NICE STREAMS (no. CTM2009-06370-E/ANT; Neogene ice streams and sedimentary processes on high-latitude continental margins, incorporated into the International Polar Year as activity no. 367), as well as the research group RNM 148 (Junta de Andalucia) and project BARACA (PID2022-136678NB-I00 AEI/FEDER, UE) and GOLETA (PID2019- 108880RJ-I00/AEI/FEDER, UE). This work represents a contribution to the CSIC Thematic Interdisciplinary Platform PTI POLARCSIC. We also thank IHS for providing the Kingdom Suite™ licence. G. Ercilla also acknowledges to IGCP 640 - S4LIDE (Significance of Modern and Ancient Submarine Slope LandSLIDEs), and to the 'Severo Ochoa Centre of Excellence' accreditation (CEX2019-000928-S).

References

Alley, R., Pollard, D., Parizek, B., Anandakrishnan, S., Pourpoint, M., Stevens, N.T., MacGregor, J.A., Christianson, K., Muto, A., Holschuh, N., 2019. Possible role for tectonics in the evolving stability of the Greenland Ice Sheet. J. Geophys. Res. Earth 124 (1), 97–115.
Alley, R.B., Blankenship, D., Rooney, S., Bentley, C., 1989. Sedimentation beneath ice shelves—the view from ice stream B. Mar. Geol. 85 (2–4), 101–120.
Anderson, E.M., 1951. The Dynamics of Faulting and Dyke Formation with Applications to Britain. Hafner Pub. Co, Edinburgh, p. 660.
Arvidsson, R., 1996. Fennoscandian earthquakes: whole crustal rupturing related to postglacial rebound. Science 274 (5288), 744–746.
Batchelor, C., Dowdeswell, J., Rignot, E., Millan, R., 2019. Submarine moraines in Southeast Greenland fjords reveal contrasting outlet-glacier behavior since the last Glacial Maximum. Geophys. Res. Lett. 46 (6), 3279–3286.
Bergh, S.G., Grogan, P., 2003. Tertiary structure of the Sørkapp-Hornsund Region, South Spitsbergen and implications for the offshore southern extension of the fold-thrust Belt. Norwegian J. Geol./Norsk Geolog. Foren. 83 (1).

Bergh, S.G., Braathen, A., Andresen, A., 1997. Interaction of basement-involved and thin-skinned tectonism in the Tertiary fold-thrust belt of Central Spitsbergen, Svalbard. AAPG Bull. 81 (4), 637–661.
Bjarnadóttir, L.R., Andreassen, K., 2016. Ice-stream landform assemblage in Kveithola, western Barents Sea margin. Geol. Soc. Lond. Mem. 46 (1), 325–328.
Bjarnadottir, L.R., Rüther, D.C., Winsborrow, M.C., Andreassen, K., 2013. Grounding-line dynamics during the last deglaciation of Kveithola, Barents Sea, as revealed by seabed geomorphology and shallow seismic stratigraphy. Boreas 42 (1), 84–107.
Bjarnadóttir, L.R., Winsborrow, M.C., Andreassen, K., 2014. Deglaciation of the Central Barents Sea. Quat. Sci. Rev. 92, 208–226.
Boulton, G., 1979. Processes of glacier erosion on different substrata. J. Glaciol. 23 (89), 15–38.
Boulton, G., Clark, C., 1990. A highly mobile Laurentide ice sheet revealed by satellite images of glacial lineations. Nature 346 (6287), 813–817.
Brandes, C., Tanner, D.C., 2014. Fault-related folding: A review of kinematic models and their application. Earth Sci. Rev. 138, 352–370.
Brekke, H., 2000. The tectonic evolution of the Norwegian Sea continental margin, with emphasis on the Voring and more basins. Spec. Public.-Geol. Soc. Lond. 167, 327–378.
Chauché, N., Hubbard, A., Gascard, J.-C., Box, J.E., Bates, R., Koppes, M., Patton, H., 2014. Ice–ocean interaction and calving front morphology at two West Greenland tidewater outlet glaciers. Cryosphere 8 (4), 1457–1468.
Clague, J.J., James, T.S., 2002. History and isostatic effects of the last ice sheet in southern British Columbia. Quat. Sci. Rev. 21 (1–3), 71–87.
Dallmann, W.K., 1993. Notes on the stratigraphy, extent and tectonic implications of the Minkinfjellet Basin, Middle Carboniferous of Central Spitsbergen. Polar Res. 12 (2), 153–160.
Dallmann, W.K., Andresen, A., Bergh, S.G., Maher Jr., H.D., Ohta, Y., 1993. Tertiary fold-and-thrust belt of Spitsbergen, Svalbard. Norsk Polarinstit.. Map Scale 1 (200), 000.
Dove, D., Evans, D.J., Lee, J.R., Roberts, D.H., Tappin, D.R., Mellett, C.L., Callard, S.L., 2017. Phased occupation and retreat of the last British–Irish Ice Sheet in the southern North Sea; geomorphic and seismostratigraphic evidence of a dynamic ice lobe. Quat. Sci. Rev. 163, 114–134.
Dowdeswell, J., Hogan, K.A., 2016. Huge iceberg ploughmarks and associated corrugation ridges on the northern Svalbard shelf. In: Atlas of Submarine Glacial Landforms: Modern, Quaternary and Ancient, vol. 46, pp. 269–270.
Dowdeswell, J.A., Villinger, H., Whittington, R.J., Marienfeld, P., 1993. Iceberg scouring in Scoresby Sund and on the East Greenland continental shelf. Mar. Geol. 111 (1–2), 37–53.
Dumais, M.A., Gernigon, L., Olesen, O., Johansen, S.E., Brönner, M., 2021. New interpretation of the spreading evolution of the Knipovich Ridge derived from aeromagnetic data. Geophys. J. Int. 224 (2), 1422–1428.
Ebinger, C.J., van Wijk, J., Keir, D., Bickford, M., 2013. The time scales of continental rifting: Implications for global processes. Geol. Soc. Am. Spec. Pap. 500, 371–396.
Elverhøi, A., Dowdeswell, J.A., Funder, S., Mangerud, J., Stein, R., 1998. Glacial and oceanic history of the Polar North Atlantic margins: an overview. Quat. Sci. Rev. 17 (1–3), 1–10.
Engen, Ø., Faleide, J.I., Dyreng, T.K., 2008. Opening of the Fram Strait gateway: A review of plate tectonic constraints. Tectonophysics 450 (1–4), 51–69.
Ercilla, G., Alonso, B., Baraza, J., Casas, D., Chiocci, F., Estrada, F., Farran, M., Gonthier, E., Perez-Belzuz, F., Pirmez, C., 1998. New high-resolution acoustic data from thebraided system'of the Orinoco deep-sea fan. Mar. Geol. 146 (1–4), 243–250.
Ercilla, G., Casas, D., Alonso, B., Casalbore, D., Galindo-Zaldívar, J., García-Gil, S., Martorelli, E., Vázquez, J.T., Azpiroz-Zabala, M., DoCouto, D., Estrada, F., Fernández-Puga, M.C., González-Castillo, L., González-Vida, J.M., Idárraga-García, J., Juan, C., Macías, J., Madarieta-Txurruka, A., Nespereira, J., Palomino, D., Sánchez-Guillamón, O., Tendero-Salmerón, V., Teixeira, M., Valencia, J., Docouto, D., 2021. Offshore geological hazards: charting the course of progress and future directions. Oceans 2, 393–428.
Estrada, F., González-Vida, J.M., Peláez, J.A., Galindo-Zaldívar, J., Ortega, S., Macías, J., Ercilla, G., 2021. Tsunami generation potential of a strike-slip fault tip in the westernmost Mediterranean. Sci. Rep. 11 (1), 16253.
Evans, D.J., 2017. Till: A Glacial Process Sedimentology. John Wiley and Sons. Inc, Hoboken, NJ, US.
Faleide, J., Gudlaugsson, S., Eldholm, O., Myhre, A., Jackson, H., 1991. Deep seismic transects across the sheared western Barents Sea-Svalbard continental margin. Tectonophysics 189 (1–4), 73–89.
Faleide, J.I., Tsikalas, F., Breivik, A.J., Mjelde, R., Ritzmann, O., Engen, Ø., Eldholm, O., 2008. Structure and evolution of the continental margin off Norway and the Barents Sea. Episod. J. Intern. Geosci. 31 (1), 82–91.
Faleide, J.I., Bjørlykke, K., Gabrielsen, R.H., 2015. Geology of the Norwegian Continental Shelf. Petroleum Geoscience: From Sedimentary Environments to Rock Physics, pp. 603–637.
Fjeldskaar, W., Lindholm, C., Dehls, J.F., Fjeldskaar, I., 2000. Postglacial uplift, neotectonics and seismicity in Fennoscandia. Quat. Sci. Rev. 19 (14–15), 1413–1422.
Friend, P.F., Harland, W.B., Rogers, D.A., Snape, I., Thornley, R.S.W., 1997. Late Silurian and early Devonian stratigraphy and probable strike-slip tectonics in northwestern Spitsbergen. Geol. Mag. 134 (4), 459–479.
Gabrielsen, R., Foersth, R., Steel, R., Idil, S., Klovjan, O., 1990. Architectural Styles of Basin Fill in the Northern Viking Graben (Paper presented at the Tectonic evolution of the North Sea rifts).
Gabrielsen, R.H., Grunnaleite, I., Rasmussen, E., 1997. Cretaceous and tertiary inversion in the Bjørnøyrenna Fault complex, South-Western Barents Sea. Mar. Pet. Geol. 14 (2), 165–178.
Gac, S., Minakov, A., Shephard, G.E., Faleide, J.I., Planke, S., 2020. Deformation analysis in the Barents Sea in relation to Paleogene transpression along the Greenland-Eurasia plate boundary. Tectonics 39 (10) e2020TC006172.
Gaina, C., Gernigon, L., Ball, P., 2009. Palaeocene–Recent plate boundaries in the NE Atlantic and the formation of the Jan Mayen microcontinent. J. Geol. Soc. Lond. 166 (4), 601–616.
García, M., Ercilla, G., Alonso, B., 2009. Morphology and sedimentary systems in the Central Bransfield Basin, Antarctic Peninsula: sedimentary dynamics from shelf to basin. Basin Res. 21 (3), 295–314.
Gomez, N., Mitrovica, J.X., Huybers, P., Clark, P.U., 2010. Sea level as a stabilizing factor for marine-ice-sheet grounding lines. Nat. Geosci. 3 (12), 850–853.
Gregersen, S., Basham, P.W., Wood, R.M., 1989. Extraordinary Deglaciation Reverse Faulting in Northern Fennoscandia. Earthquakes at North-Atlantic Passive Margins: Neotectonics and Postglacial Rebound, pp. 141–173.
Hampel, A., 2017. Response of faults to climate-induced changes of ice sheets, glaciers and lakes. Geol. Today 33 (1), 12–18.
Hampel, A., Hetzel, R., 2006. Response of normal faults to glacial-interglacial fluctuations of ice and water masses on Earth's surface. J. Geophys. Res. Solid Earth 111 (B6).
Heidbach, O., Rajabi, M., Reiter, K., Ziegler, M., Wsm Team, 2016. World stress map database release 2016. In: GFZ Data Services, vol. 10.
Hetzel, R., Hampel, A., 2005. Slip rate variations on normal faults during glacial–interglacial changes in surface loads. Nature 435 (7038), 81–84.
Hoffman, P., 2016. Cryoconite pans on Snowball Earth: supraglacial oases for Cryogenian eukaryotes? Geobiology 14 (6), 531–542.
Ingólfsson, Ó., Norddahl, H., 2001. High relative sea level during the Bolling Interstadial in western Iceland: a reflection of ice-sheet collapse and extremely rapid glacial unloading. Arct. Antarct. Alp. Res. 33 (2), 231–243.
Jakobsson, M., Backman, J., Rudels, B., Nycander, J., Frank, M., Mayer, L., Jokat, W., Sangiorgi, F., O'Regan, M., Brinkhuis, H., 2007. The early Miocene onset of a ventilated circulation regime in the Arctic Ocean. Nature 447 (7147), 986–990.
Jakobsson, M., Anderson, J.B., Nitsche, F.O., Dowdeswell, J.A., Gyllencreutz, R., Kirchner, N., Majewski, W., 2011. Geological record of ice shelf break-up and grounding line retreat, Pine Island Bay, West Antarctica. Geology 39 (7), 691–694.
Jakobsson, M., Mayer, L., Coakley, B., Dowdeswell, J.A., Forbes, S., Fridman, B., Rebesco, M., 2012. The international bathymetric chart of the Arctic Ocean (IBCAO) version 3.0. Geophys. Res. Lett. 39 (12).
Japsen, P., Chalmers, J.A., 2000. Neogene uplift and tectonics around the North Atlantic: overview. Glob. Planet. Chang. 24 (3–4), 165–173.
Johnson, H. (Ed.), 2008. The Nature and Origin of Compression in Passive Margins. Geological Society of London.
Jokat, W., O'Connor, J., Hauff, F., Koppers, A.A., Miggins, D.P., 2019. Ultraslow spreading and volcanism at the eastern end of Gakkel Ridge, Arctic Ocean. Geochem. Geophys. Geosyst. 20 (12), 6033–6050.
Junek, W.N., Roman-Nieves, J.I., Woods, M.T., 2014. Tectonic implications of earthquake mechanisms in Svalbard. Geophys. J. Int. 196 (2), 1152–1161.
Keiding, M., Kreemer, C., Lindholm, C., Gradmann, S., Olesen, O., Kierulf, H., 2015. A comparison of strain rates and seismicity for Fennoscandia: depth dependency of deformation from glacial isostatic adjustment. Geophys. J. Int. 202 (2), 1021–1028.
Klemann, V., Wolf, D., 1998. Modelling of stresses in the Fennoscandian lithosphere induced by Pleistocene glaciations. Tectonophysics 294 (3–4), 291–303.
Knies, J., Matthiessen, J., Vogt, C., Laberg, J.S., Hjelstuen, B.O., Smelror, M., Vorren, T. O., 2009. The Plio-Pleistocene glaciation of the Barents Sea–Svalbard region: a new model based on revised chronostratigraphy. Quat. Sci. Rev. 28 (9–10), 812–829.
Kristoffersen, Y., 1990. On the Tectonic Evolution and Paleoceanographic Significance of the Fram Strait Gateway. Geological History of the Polar Oceans: Arctic versus Antarctic, pp. 63–76.
Kukkonen, I.T., Ask, M.V., Olesen, O., 2011. Postglacial fault drilling in northern Europe: Workshop in Skokloster, Sweden. Sci. Drill. 11, 56–59.
Łącka, M., Zajączkowski, M., Forwick, M., Szczuciński, W., 2015. Late Weichselian and Holocene paleoceanography of Storfjordrenna, southern Svalbard. Clim. Past Discuss. 10 (4).
Lagerbäck, R., Sundh, M., 2008. Early Holocene Faulting and Paleoseismicity in Northern Sweden, 836. Sveriges geologiska undersökning—Research paper, Uppsala, Sweden.
Lambeck, K., Yokoyama, Y., Purcell, T., 2002a. Into and out of the last Glacial Maximum: sea-level change during Oxygen Isotope Stages 3 and 2. Quat. Sci. Rev. 21 (1–3), 343–360.
Lambeck, K., Esat, T.M., Potter, E.K., 2002b. Links between climate and sea levels for the past three million years. Nature 419 (6903), 199–206.
Lasabuda, A., Laberg, J.S., Knutsen, S.M., Safronova, P., 2018. Cenozoic tectonostratigraphy and pre-glacial erosion: A mass-balance study of the northwestern Barents Sea margin, Norwegian Arctic. J. Geodyn. 119, 149–166.
Lasabuda, A.P., Johansen, N.S., Laberg, J.S., Faleide, J.I., Senger, K., Rydningen, T.A., Hanssen, A., 2021. Cenozoic uplift and erosion of the Norwegian Barents Shelf–A review. Earth Sci. Rev. 217, 103609.
Lindblom, E., Lund, B., Tryggvason, A., Uski, M., Bödvarsson, R., Juhlin, C., Roberts, R., 2015. Microearthquakes illuminate the deep structure of the endglacial Pärvie fault, northern Sweden. Geophys. J. Int. 201 (3), 1704–1716.
Lønne, I., Nemec, W., 2011. Modes of sediment delivery to the grounding line of a fast-flowing tidewater glacier: implications for ice-margin conditions and glacier dynamics. Geol. Soc. Lond. Spec. Publ. 354 (1), 33–56.
Løseth, H., Henriksen, S., 2005. A Middle to Late Miocene Compression Phase along the Norwegian Passive Margin. Geological Society, London (Petroleum Geology Conference Series.).

Lucchi, R.G., Sagnotti, L., Camerlenghi, A., Macrì, P., Rebesco, M., Pedrosa, M.T., Giorgetti, G., 2015. Marine sedimentary record of Meltwater Pulse 1a along the NW Barents Sea continental margin. arktos 1, 1–14.
Malehmir, A., Socco, L.V., Bastani, M., Krawczyk, C.M., Pfaffhuber, A.A., Miller, R.D., Bazin, S., 2016. Near-surface geophysical characterization of areas prone to natural hazards: a review of the current and perspective on the future. Adv. Geophys. 57, 51–146.
Maslin, M., Owen, M., Day, S., Long, D., 2004. Linking continental-slope failures and climate change: Testing the clathrate gun hypothesis. Geology 32 (1), 53–56.
Minakov, A., Yarushina, V., Faleide, J.I., Krupnova, N., Sakoulina, T., Dergunov, N., Glebovsky, V., 2018. Dyke emplacement and crustal structure within a continental large igneous province, northern Barents Sea. Geol. Soc. Lond. Spec. Publ. 460 (1), 371–395.
Mitchell, B., Bungum, H., Chan, W., Mitchell, P., 1990. Seismicity and present-day tectonics of the Svalbard region. Geophys. J. Int. 102 (1), 139–149.
Myhre, A.M., Eldholm, O., 1988. The western Svalbard margin (74–80 N). Mar. Pet. Geol. 5 (2), 134–156.
Nielsen, T., Rasmussen, T.L., 2018. Reconstruction of ice sheet retreat after the last Glacial maximum in Storfjorden, southern Svalbard. Mar. Geol. 402, 228–243.
Olesen, O., Ebbing, J., Lundin, E., Mauring, E., Skilbrei, J., Torsvik, T., Sand, M., 2007. An improved tectonic model for the Eocene opening of the Norwegian–Greenland Sea: Use of modern magnetic data. Mar. Pet. Geol. 24 (1), 53–66.
Ottesen, D., Dowdeswell, J.A., 2022. Distinctive iceberg ploughmarks on the mid-Norwegian margin: Tidally influenced chains of pits with implications for iceberg drift. Arct. Antarct. Alp. Res. 54 (1), 163–175.
Ottesen, D.A.G., Dowdeswell, J.A., Landvik, J.Y., Mienert, J., 2007. Dynamics of the late Weichselian ice sheet on Svalbard inferred from high-resolution sea-floor morphology. Boreas 36 (3), 286–306.
Patton, H., Hubbard, A., Heyman, J., Alexandropoulou, N., Lasabuda, A.P., Stroeven, A. P., Andreassen, K., 2022. The extreme yet transient nature of glacial erosion. Nat. Commun. 13 (1), 7377.
Paxman, G.J., Jamieson, S.S., Ferraccioli, F., Bentley, M.J., Forsberg, R., Ross, N., Watts, A.B., Corr, H.F.J., Jordan, T.A., 2017. Uplift and tilting of the Shackleton Range in East Antarctica driven by glacial erosion and normal faulting. J. Geophys. Res. Solid Earth 122 (3), 2390–2408.
Pedrosa, M., Camerlenghi, A., De Mol, B., Urgeles, R., Rebesco, M., Lucchi, R.G., 2011. Seabed morphology and shallow sedimentary structure of the Storfjorden and Kveithola trough-mouth fans (North West Barents Sea). Mar. Geol. 286 (1–4), 65–81.
Pedrosa-González, M.T., González-Vida, J.M., Galindo-Záldivar, J., Ortega, S., Castro, M. J., Casas, D., Ercilla, G., 2022. Simulation of tsunami induced by a submarine landslide in a glaciomarine margin: the case of Storfjorden LS-1 (southwestern Svalbard Islands). Nat. Hazards Earth Syst. Sci. 22 (12), 3839–3858.
Pfirman, S.L., Solheim, A., 1989. Subglacial meltwater discharge in the open-marine tidewater glacier environment: observations from Nordaustlandet, Svalbard Archipelago. Mar. Geol. 86 (4), 265–281.
Piotrowski, J.A., Larsen, N.K., Menzies, J., Wysota, W., 2006. Formation of subglacial till under transient bed conditions: deposition, deformation and basal decoupling under a Weichselian ice sheet lobe, Central Poland. Sedimentology 53 (1), 83–106.
Pirli, M., Schweitzer, J., Paulsen, B., 2013. The Storfjorden, Svalbard, 2008–2012 aftershock sequence: Seismotectonics in a polar environment. Tectonophysics 601, 192–205.
Pirli, M., Schweitzer, J., Paulsen, B., Konechnaya, Y.V., Antonovskaya, G.N., 2021. Two decades of seismicity in Storfjorden, Svalbard archipelago, from regional data. Seismol. Res. Lett. 92 (5), 2695–2704.
Powell, R., Domack, G.W., 2002. Modern Glaciomarine Environments Modern and Past Glacial Environments. Elsevier, pp. 361–389.
Powell, R., Evans, J.A., 1983. A new geobarometer for the assemblage biotite-muscovite-chlorite-quartz. J. Metamorph. Geol. 1 (4), 331–336.
Rebesco, M., Liu, Y., Camerlenghi, A., Winsborrow, M., Laberg, J.S., Caburlotto, A., Wardell, N., 2011. Deglaciation of the western margin of the Barents Sea Ice Sheet—A swath bathymetric and sub-bottom seismic study from the Kveithola Trough. Mar. Geol. 279 (1–4), 141–147.
Rebesco, M., Laberg, J., Pedrosa, M., Camerlenghi, A., Lucchi, R., Zgur, F., Wardell, N., 2014. Onset and growth of trough-mouth fans on the North-Western Barents Sea margin–implications for the evolution of the Barents Sea/Svalbard ice sheet. Quat. Sci. Rev. 92, 227–234.
Rüther, D.C., Bjarnadóttir, L.R., Junttila, J., Husum, K., Rasmussen, T.L., Lucchi, R.G., Andreassen, K., 2012. Pattern and timing of the northwestern B arents S ea I ce S heet deglaciation and indications of episodic H olocene deposition. Boreas 41 (3), 494–512.
Shackleton, C.S., Winsborrow, M.C., Reassen, K., Lucchi, R.G., Bjarnadóttir, L.R., 2019. Ice-margin retreat and grounding-zone dynamics during initial deglaciation of the Storfjordrenna Ice Stream, western Barents Sea. Boreas 49 (1), 38–51.
Srivastava, S., 1985. Evolution of the Eurasian Basin and its implications to the motion of Greenland along Nares Strait. Tectonophysics 114 (1–4), 29–53.
Stange, S., Schweitzer, J., 2004. Source depths at regional distances: an example from the western Barents Sea/Svalbard region. NORSAR Scient. Report 1 (2004), 45–50.
Steffen, H., Olesen, O., Sutinen, R., 2021. Glacially triggered faulting: A historical overview and recent developments. In: Steffen, H., Olesen, O., Sutinen, R. (Eds.), Glacially-Triggered Faulting. Cambridge University Press, Cambridge, p. 3e19. https://doi.org/10.1017/9781108779906.003.
Stewart, I.S., Sauber, J., Rose, J., 2000. Glacio-seismotectonics: ice sheets, crustal deformation and seismicity. Quat. Sci. Rev. 19 (14–15), 1367–1389.
Stokes, C., Spagnolo, M., Clark, C., Cofaigh, C.Ó., Lian, O., Dunstone, R., 2013. Formation of mega-scale glacial lineations on the Dubawnt Lake Ice Stream bed: 1. Size, shape and spacing from a large remote sensing dataset. Quat. Sci. Rev. 77, 190–209.
Stokes, C.R., Clark, C.D., 2003. Laurentide ice streaming on the Canadian Shield: A conflict with the soft-bedded ice stream paradigm? Geology 31 (4), 347–350.
Talwani, M., Eldholm, O., 1977. Evolution of the Norwegian-Greenland Sea. Geol. Soc. Am. Bull. 88 (7), 969–999.
Turpeinen, H., Hampel, A., Karow, T., Maniatis, G., 2008. Effect of ice sheet growth and melting on the slip evolution of thrust faults. Earth Planet. Sci. Lett. 269 (1–2), 230–241.
Vincenz, S., Jeleńska, M., Aiinehsazian, K., Birkenmajer, K., 1984. Palaeomagnetism of some late Mesozoic dolerite sills of east Central Spitsbergen, Svalbard Archipelago. Geophys. J. Int. 78 (3), 751–773.
Vorren, T.O., Landvik, J.Y., Reassen, K., Laberg, J.S., 2011. Glacial History of the Barents Sea Region Developments in Quaternary Sciences, vol. 15. Elsevier, pp. 361–372.
Watts, A.B., 2001. Isostasy and Flexure of the Lithosphere. Cambridge University Press, Cambridge, p. 458.
Wellner, J.S., Lowe, A.L., Shipp, S.S., Anderson, J.B., 2001. Distribution of glacial geomorphic features on the Antarctic continental shelf and correlation with substrate: implications for ice behavior. J. Glaciol. 47 (158), 397–411.
Wells, D.L., Coppersmith, K.J., 1994. New empirical relationships among magnitude, rupture length, rupture width, rupture area and surface displacement. Bull. Seismol. Soc. Am. 84 (4), 974–1002.
Whitehouse, P.L., Gomez, N., King, M.A., Wiens, D.A., 2019. Solid Earth change and the evolution of the Antarctic Ice Sheet. Nat. Commun. 10 (1), 503.
Winsborrow, M.C., Andreassen, K., Corner, G.D., Laberg, J.S., 2010. Deglaciation of a marine-based ice sheet: late Weichselian palaeo-ice dynamics and retreat in the southern Barents Sea reconstructed from onshore and offshore glacial geomorphology. Quat. Sci. Rev. 29 (3–4), 424–442.
Winsnes, T.S., Birkenmajer, K., Dallmann, W.K., Hjelle, A., Salvigsen, O., 1993. Geologi–Cal Map of Svalbard 1: 100,000. Sheet C13 Sørkapp. Map Part. Norsk Polarinstitutt, Oslo.
Wise, M.G., Dowdeswell, J.A., Jakobsson, M., Larter, R.D., 2017. Evidence of marine ice-cliff instability in Pine Island Bay from iceberg-keel plough marks. Nature 550 (7677), 506–510.
Zecchin, M., Rebesco, M., 2018. Glacigenic and glacimarine sedimentation from shelf to trough settings in the NW Barents Sea. Mar. Geol. 402, 184–193.